Spin Textures in High Aspect Ratio $Ni_{80}Fe_{20}$ Nanodisk Arrays: Implications for Next-Generation Spintronic Devices

M S Devapriya[1], Xue Zhou[2], Arabinda Haldar[1*], Adekunle Olusola Adeyeye[2,3#]

[1]*Department of Physics, Indian Institute of Technology Hyderabad, Kandi 502284, Telangana, India*

[2]*Department of Electrical and Computer Engineering, National University of Singapore, Singapore 117576*

[3]*Department of Physics, Durham University, South Road, Durham DH1 3LE, United Kingdom*

Corresponding authors: [*]arabinda@phy.iith.ac.in, [#]adekunle.o.adeyeye@durham.ac.uk

ABSTRACT

Recent progress in nanomagnetism has generated significant enthusiasm for the creation of high-aspect-ratio nanostructures. Nonetheless, fabricating large-area thick nanostructures encounters substantial hurdles due to inherent lithographic constraints. In this study, we showcase the fabrication of magnetic nanodisks patterned with deep UV, reaching thicknesses of up to 200 nm, accomplished through the creation of nano trenches in the Si substrate. Subsequently, the evolution of spin texture and spin dynamics as a function of thickness (20 – 200 nm) have been presented. The magnetization reversal studies reveal that the disks have a vortex as their ground state configuration—the nucleation and annihilation fields associated with the vortex increase with increasing thickness. We observe an increase in vortex core diameter as the disk thickness is increased. Micromagnetic simulations suggest the presence of an out-of-plane magnetization component is observed along the circumference, in addition to the into-the-plane magnetization at the center for disks of higher thicknesses. The magnetization dynamics studies reveal that the center mode frequency increases with increasing thickness, and there is a mirror symmetry in the excitation amplitude between the top and bottom layers for nanodisks with thickness greater than 50 nm. The results are substantiated with micromagnetic simulations. Our results open horizons in the utilization of the third dimension for emerging spin textures and their potential applications in future spintronic devices.

Keywords: Thick nanodisks, Magnetization dynamics, Ferromagnetic resonance, Micromagnetic simulations, deep UV lithography, Spin textures, Nanomagnetism, Spintronics

1. INTRODUCTION

Nanomagnets are the elementary blocks of energy-efficient, non-volatile spintronic devices. Nanowires, nanorings, and nanodots are some of the most extensively explored nanostructures for various technologies. For instance, domain walls in nanowires/nanostripes are shown to be suitable for racetrack memory applications (1–4). The two equilibrium states in ferromagnetic nanorings, the vortex and the onion state (5,6) are being explored for magnetic sensors and memory (7–9). Both these vortex and onion states also demonstrate rich spin dynamics (10,11). Among these patterned nanostructures, nanodots/nanodisks have been studied extensively due to the presence of vortex configuration at remanence (12) and configurational anisotropy (13). Owing to these properties, nanodots find applications in magnetic sensors and magnetic logic (13), magnetic random-access memory (14), and spin torque nano oscillators (15).

Most of the research has primarily focused on two-dimensional (2D) planar nanostructures where the film thickness is significantly smaller than the planar dimensions. With advances in nanofabrication techniques and the increasing demand in the field, researchers have started to exploit the effect of film thickness towards 3D nanomagnetism (16–20). To the best of our knowledge, experimental studies have been conducted in lithographically defined circular nanodots with thicknesses up to 100 nm(21–29). The remanent state of a nanodot with a suitable aspect ratio (the ratio of thickness to radius) is a vortex structure(30) and it has been found to have rich spin dynamics in initial experiments(31). However, the studies were mostly limited to vortex excitations, which are uniform in thickness. The vortex modes with non-uniform excitation along the thickness were first experimentally observed by J. Ding et al. (24,25). The uniform gyrotropic mode exhibits an increasing phase difference between top and bottom surfaces with thickness, thus reducing intensity. Interestingly, the phase difference for the first-order gyrotropic mode decreases with thickness, resulting in an increased intensity than the uniform gyrotropic modes at higher thicknesses. Moreover, these higher-order

gyrotropic modes lie in the gigahertz frequency range, making them a potential candidate for spin torque oscillator-based applications(27). In nanodisks of thickness 120 nm, a superimposition of a skyrmion, a vortex, and a meron pair has been observed(21). The core of these structures dilates with increasing thickness. The presence of these chiral structures can help in the design of topologically protected memory elements. Compared to planar nanodots, the model for thicker nanodots includes a mass term (inertia term) to the vortex equation of motion(26). Spin wave modes were also detected in a perpendicularly magnetized thick nanodot array. An axially antisymmetric mode is observed in these thick dots due to the non-uniform excitation along the thickness(22). Deep UV (DUV) lithography has emerged as a viable method for large-area patterns(32). However, patterning large aspect ratio nanostructures remains a significant challenge for both e-beam and DUV lithography techniques that involve a lift-off process. In this study, we use the DUV lithography technique to first etch nano trenches with a depth of approximately 300 nm, followed by the deposition of magnetic materials. This innovative method ensures geometrical integrity along the thickness for thick nanostructures across a large area pattern. While a few investigations have been conducted on nanodisks up to an aspect ratio of 0.6 (21,25), a systematic study on the impact of much higher thickness on spin configurations and dynamics remains elusive.

Here, we report a comprehensive study on the effect of disk thickness on the magnetization reversal and dynamic responses of circular nanodisks of a fixed diameter of 450 nm and thickness in the range from 20 nm to 200 nm. To eliminate the edge roughness inherent in the lift-off process, we have developed an innovative lithographic technique to create nano-trenches into the Si-substrate, followed by the deposition of permalloy film of various thicknesses into these nano-channels. A detailed micromagnetic simulation study was also conducted to enhance our understanding of the reversal mechanism and dynamic processes. We observed that vortex nucleation and annihilation fields, vortex core diameter, resonance

frequencies, and linewidth are highly sensitive to the disks' thickness. We report the emergence of some unconventional spin distributions at higher thicknesses. We also observed an amplitude inversion in excitations of nanodisks' top and bottom faces for thicker nanodisks.

2. MICROMAGNETIC SIMULATIONS

The micromagnetic simulations were performed using an ordinary differential equation solver called Object Oriented Micromagnetic Framework (OOMMF)(33). Standard parameters of Py(34) are used in the simulations: saturation magnetization (M_S) = 8 × 10^5 A/m, exchange constant (A) = 13 × 10^{-12} J/m, damping constant (α) = 0.008, magneto crystalline anisotropy (K) = 0. A cuboidal cell size of 5×5×5 nm^3 was chosen considering the exchange length defined by $l_{ex} = \sqrt{\frac{2A}{M_S^2 \mu_0}}$ of Py (~5.7 nm). We have assumed a higher damping constant value (α = 0.5) to accelerate the run time and obtain remanent states without significantly affecting the results(35).

Figure 1a shows the simulated remanence spin configuration of a permalloy nanodisk of diameter, D = 450 nm and thickness t = 200 nm. The out-of-plane (OOP) magnetization component, m_z, is colour-coded for the top, middle, and bottom layers. We observe that the core diameter is dilated. In addition to the into-the-plane magnetization at the disk's center, an OOP magnetization is also observed at the peripheral region in the middle layer. It is also to be noted that there is a variation in the spin configuration across the thickness. Figure 1b shows the variation of remanent in-plane (IP) (m_x) and OOP (m_z) magnetization states for the top, middle, and bottom layers of disks as a function of film thicknesses. Conventional vortices are characterized by zero net magnetization with no radial components. Non-zero radial magnetic components can result in volume charges and hence be energetically unfavourable. It is clear from the figure that for t = 20 nm-thick nanodisks, the remanent state is a conventional vortex with zero radial components. The m_x distribution shows that the middle layer of every thickness

behaves like a conventional vortex. However, we observed a significant variation in the m_x distribution across the thickness, from thickness t = 100 nm. This originates from the search for optimal flux closure between the surface charges (34). It is also noted that surface layers appear to be mirror images of each other. The m_z distribution also changes across the thickness. As evident from figure 1b, the effect of thickness on m_z is notably prominent in the middle layer of the disk. We observe a marked increase in the vortex core diameter with the thickness from 45 nm for a 20 nm thick disk to 210 nm for a 200 nm thick disk. The vortex core radius is highly dependent on the z coordinate. Maximum dilation is observed at the middle layer and minimum at the surface layers (bottle-neck effect (34)). We also observe the presence of a non-zero OOP magnetization component near the peripheral region for t = 170 and 200 nm, as shown in figure 1b. ~~This kind of antiparallel arrangement is generally associated with skyrmion.~~ Similar kinds of unconventional spin distributions were reported in previous studies (21,36). To understand the variation of magnetization components across the layers, we performed a line scan across the thickness and diameter of the disks. Figures 1c-d depict the variation of m_x and m_z as a function of layer number for a single spin close to the center (across the dotted lines as shown in figure 1a for different thicknesses of disks). We observe that the value of m_x changes through the layers for thicker nanodisks. This behaviour is different from the conventional vortices. It is evident from the figure that the net magnetization is zero at the middle layers and attains a finite value when moving away from the middle layers. This suggests the presence of some net divergence in the surface layers of the disk. The phase difference of m_x between the top and bottom layers decreases with decreasing thickness. The nanodisk with the least thickness (t = 20 nm) does not exhibit any change in m_x throughout its thickness and is almost close to zero. This behaviour corresponds to a typical vortex.

Similarly, the OOP magnetization component, m_z, exhibits variations across the thickness with a decrease in the m_z value with the decrease in the thickness. The difference between the central

and outer layers is significant at higher thicknesses. The m_z value is maximum at the middle layer and minimum at the exterior layers. As expected, the value of m_z is almost negligible for a 20 nm thick disk. We also carried out a horizontal scan across the middle layer (dotted lines shown in figure 1a for various thicknesses. Figures 1e-f represent the variation of m_x and m_z across the diameter for the middle layer, respectively. Figure 1e clearly shows the dilation in vortex diameter with the increase in thickness. We also notice that the OOP component gradually increases and exhibits a sign change at the peripheral region for t = 170 and 200 nm. As shown in figure 1f, the value of m_x along the diameter is negligible for t = 200 nm, and it increases with decreasing thickness. This can also be a consequence of vortex core dilation. The evolution of magnetization states with the magnetic field is also interesting at higher thicknesses. We have observed the vortex displacement away from the center and its annihilation at higher fields. It is found that there is a net OOP magnetic moment, even at the saturation field (see supplementary figure. S1 for more information). Similar to the remanent states, the magnetization configuration of the surface layers are mirror images of each other. This behaviour, even at the saturation fields, makes them more interesting for conducting in-depth investigations into their fundamental properties.

3. SAMPLE PREPARATION AND EXPERIMENTAL SETUP

We have investigated the role of film thickness on nanodisks' static and dynamic behaviour experimentally. Periodic arrays of circular holes with diameter d = 450 nm and pitch p = 725 nm were patterned on Si substrate over a large area (4 mm x 4 mm) using deep ultraviolet lithography at 248 nm exposure wavelength. The circular holes were first defined on 280 nm thick positive photoresist on top of 60 nm thick bottom anti-reflective coating (BARC). Details of the processing steps can be found elsewhere(32). After resist development, the BARC layer was etched at a rate of 7Å/sec in O_2 (5 sccm) plasma heavily diluted with Argon (45 sccm). The resist circular hole structures were transferred into silicon using a mixture of C_4F_8 (10

sccm) and SF_6 (40 sccm) gas plasma. A 300 nm deep silicon was etched in plasma with vertical sidewalls and extremely good selectivity between Si and the DUV resist, which act as an etch mask. $Ni_{80}Fe_{20}$ film with thicknesses in the range from 20nm to 200nm was then deposited on the patterned substrate using an electron beam evaporation technique in a chamber with a base pressure of $2x10^{-8}$ Torr followed by lift-off process, resulting in arrays of $Ni_{80}Fe_{20}$ disks embedded in the silicon. The fabricated samples were imaged using a field emission scanning electron microscope (FESEM) to evaluate the quality of fabrication. Depth profiles of the samples were analyzed using atomic force microscopy (AFM). The magnetization reversal in nanodots was studied using a vibrating sample magnetometer (VSM) in an in-plane and out-of-plane geometry. The magnetic field was swept from +600 mT to -600 mT in a field step of 2 mT. The magnetization dynamics were probed using lock-in-based broadband ferromagnetic resonance (FMR) spectroscopy at room temperature. The samples were placed over a coplanar waveguide in a flip-chip configuration, with an oscillating microwave field, h_{rf}, applied perpendicular to the coplanar waveguide (CPW). The FMR spectra are acquired for excitation frequencies from 3-18 GHz with a step of 0.5 GHz by sweeping the magnetic field from +300 mT to −300 mT with a step of 0.2 mT. The derivative of absorption power with respect to the applied magnetic field (H_a) is then measured using a lock-in amplifier, where H_a is modulated at the reference frequency (490 Hz) using a Helmholtz coil. Figure 2a provides a schematic illustration of our fabrication process. Figure 2b shows the FESEM images of nanodisk arrays of D = 450 nm and disk-to-disk separation, s = 500 nm, with varying thicknesses from 20 nm to 200 nm. Since Py is deposited into the etched holes of silicon, we observe an increase in contrast with the increasing thickness of the disks. The depth profile of the holes filled with Py is shown in figure 2c. For illustrations, the line scans indicate the depth profiles across three adjacent disks (marked by a dotted line). Lower depths refer to the higher thickness of the Py nanodisks. The depth profile values from AFM may not be exact due to the interaction of the

AFM tip with the walls of the trenches, and hence, they should be used as a qualitative representation of the trench profiles post-filling the magnetic materials.

4. RESULTS AND DISCUSSION

4.1. Magnetization reversal:

To investigate the effect of the substantially large thicknesses of the nanodisks, we have recorded the magnetization reversal processes using the VSM. Figure 3a shows the magnetization reversal curves for various thicknesses ranging from 20 – 200 nm in an IP configuration. The hysteresis loops contain two triangular lobes, similar to typical nanodisks with vortex as a ground state configuration for nanodisks for $t < 50$ nm(37). The sudden decrease in the average magnetization of nanodisks, with the reduction of the magnetic field and negligible coercivity, indicates the presence of a vortex. The formation of a vortex involves the competition between magnetostatic energy and exchange energy. As we decrease the field, the vortex nucleated at the end of the nanodisk gets displaced towards the center and reaches the center at zero magnetic fields. With further reduction in the field, the magnetic vortex becomes unstable and annihilates to form a single-domain state. The nucleation and annihilation fields are marked in the IP hysteresis loop using violet and green arrows, respectively. It is evident from the hysteresis loops that vortex nucleation and annihilation fields are highly dependent on thickness. These fields increase with film thickness. A slanted hysteresis is observed for samples with higher thicknesses due to the evolution of complex spin textures. The slight hysteresis at the remanence may be due to sample defects(38). Due to the high aspect ratios of the nanodisks, magnetization reversals were also measured in an OOP configuration, as shown in figure 3b for all the thicknesses. The nanodisks favour an OOP magnetic configuration at higher thicknesses. The increasing shape anisotropy and demagnetization effects aligned the magnetic moments to align along their thickness. The

simulated hysteresis loops for IP and OOP configuration (see supplementary figure S2 for more information) substantiate our experimental findings with reasonable lithographic fabrication-based slight deviation limits. To visualize the magnetic configurations, we performed magnetic force microscopy (MFM) experiments at remanence for D = 170 nm and D = 200 nm arrays (figures 3c-f). We recorded the MFM images at remanence from two different initialization processes: saturating magnetic field applied in the OOP and IP directions. We observed a large vortex core for all the nanodisks at remanence, which is much larger than a conventional vortex core diameter (~ 50 nm) in a thin circular disk. On the other hand, the polarity of the vortex core is uniform when initialized with the OOP magnetic field. However, the polarities of the cores are random in the IP field initialized case. The MFM images shed light on the possibility of the evolution of complex spin textures with the increase in thickness. The elliptical nature of MFM of disks in MFM images is due to the drifts that occurred during the scan. We could not obtain MFM images for the lower thicknesses as these nanodisks are deep inside the etched holes, which were difficult to access using the scanning probe tip.

4.2. Magnetization dynamics:

The magnetization dynamics were probed using lock-in-based broadband FMR technique. Figure 4a shows the representative FMR spectra at 12 GHz for different thicknesses of nanodisk arrays. We observe an intense mode and multiple modes with weak intensity for the 20-nm-thick nanodisks. The resonance field ($\mu_0 H_r$) of the high-intensity mode exhibits a strong sensitivity to the thickness. It increases with increasing thickness. The absence of weak intensity modes in samples with thicknesses greater than 20 nm may be due to weak excitation,

and it is beyond our FMR detection limit. We also observe a splitting in the high-intensity mode for 200 nm thick disks.

We have carried out a detailed micromagnetic simulation to understand more about the spin dynamics of nanodisk arrays. The simulations were performed for an array of nanodisks, with an external magnetic field applied along the x-axis and the *sinc* pulse along the y-axis, similar to our experimental setup. To simulate FMR modes, a sinc pulse is defined as $h_{rf} = h_0 \frac{\sin(2\pi f_c \tau')}{2\pi f_c \tau'}$, where the amplitude of sinc wave $h_0 = 5$ mT, cutoff frequency $f_c = 19$ GHz, and $\tau' = \tau - \tau_0$ refers to the simulation time (τ) with an offset τ_0. Sinc pulse is applied perpendicular to the biasing field (along the y-axis) to maximize the torque. Dynamic simulations are carried out for a time period of 4 ns with a sampling time of 10 ps. The dynamic magnetization data are post-processed in the frequency domain using the fast Fourier transform (FFT) procedure to obtain FMR modes. We have analyzed magnetization as a function of position and time, i.e., M = M (x, y, z, t), to obtain the spatial FMR mode profiles.

The simulated FMR spectra corresponding to each mode of a 20 nm thick sample are shown in figure 4b. The simulations were carried out at different magnetic fields, corresponding to the $\mu_0 H_r$ value of each mode. 2D spatial profiles of the modes corresponding to each mode are also included in figure 4b. The red and blue colour indicates maximum and minimum absorption, respectively. The '♦' (at 11.3 GHz) labelled mode, with maximum intensity in the experimental FMR spectra, is identified as the center mode (CM). The spatial profiles of this mode reveal that it has maximum absorption at the center of the nanodisk. Two other low-intensity modes are also observed very close to the CM. These '▲' (at 12 GHz) and '▼' (at 12 GHz) labelled modes also show maximum absorption at the center. A very low-intensity, high linewidth mode is also identified far away from the CM. The spatial profile of these '●' (at 12.4 GHz) labelled modes indicates its maximum excitation at the edges and is hence identified as the edge modes

(EM). The EM appears at a higher field and has a broader linewidth. The mode profiles of high-intensity mode in the FMR spectra of the nanodisks along the top, middle, and bottom surfaces are shown in figure 4c. It is observed that at lower thicknesses, i.e., 20 nm and 50 nm, the profiles of nanodisks are identical for the three surfaces, indicating uniform excitations along the thickness. Non-uniform excitations are observed for disk arrays at higher thicknesses. The top and bottom surface mode profiles are in mirror symmetry. The amplitude of the mode profiles is inverted for higher thicknesses. It is observed that the surface layers of t = 200 nm disks exhibit inhomogeneities in their static magnetization profiles at the saturation state (see supplementary information figure S1). Similar behaviour is observed for disks with t > 50 nm. The amplitude inversion of spatial mode profiles can be attributed to these inhomogeneities in the static magnetization profiles.

Figure 5a describes the two-dimensional contour plots of the FMR spectra for various thicknesses of nanodisk arrays obtained from both experiments and simulations. The contour plot is generated from the individual FMR data acquired at a given frequency by sweeping the magnetic field. The intense modes in the contour plot are observed beyond the saturation field for the samples. Hence, these modes correspond to the n = 0 modes, where magnetization precession is uniform along the thickness (25). It is to be noted that our simulation data is consistent with our experiments. The slight deviations can be attributed to the slight variations in the diameter of the nanodisks during the lithographic fabrication process. We have observed the disappearance of the FMR response in the vicinity of the zero-field region. Similar behaviour is also found in the simulated FMR spectra. The field range lies between the nucleation and annihilation fields of the vortex for every film thickness. Hence, this region, devoid of FMR response, might be associated with the formation and displacement of a magnetic vortex. The difference in the magnetic field in the area where FMR mode is absent is defined as $\mu_0 \Delta H_{gap}$. The variation of $\mu_0 \Delta H_{gap}$ with the thickness is plotted in figure 5b. $\mu_0 \Delta H_{gap}$

linearly increases with thickness. This increase in $\mu_0\Delta H_{gap}$ is associated with increased nucleation and annihilation fields with thickness, as observed in the magnetization reversal studies. The magnetization slowly curls around the center, forming a vortex structure at zero magnetic field. The effective field in this region is non-uniform, and hence, multiple modes are observed. The intensity of these modes is very weak, which makes their detection challenging.

We have extracted the values of $\mu_0 H_r$ by fitting the raw FMR spectra using a derivative Lorentzian function for all frequencies. The extracted values of $\mu_0 H_r$ for different thicknesses are shown in figure 5c. The FMR response of the nanodisk arrays with the applied field is well explained using the Kittel formula(39):

$$f = \frac{\gamma \mu_0}{2\pi} \sqrt{[H_a + (N_z - N_x).M_s][H_a + (N_y - N_x).M_s]} \quad (1)$$

where $\frac{\gamma}{2\pi} = 28.02$ GHz/T, μ_0 is the magnetic permeability, and N_x, N_y, N_z are the demagnetizing factors along the *x, y,* and *z* directions, respectively. Here, as we use a circular nanodisk $N_x = N_y$ and $N_x+N_y+N_z = 1$. The solid line in Figure 5c corresponds to the fitting of our experimental data with Equation 1. We have also extracted the demagnetizing factors from the corresponding fit. The demagnetizing factor N_z increases with increasing thickness. The increase in $\mu_0 H_r$ with thickness can be attributed to this increase in N_z.

5. CONCLUSION

In summary, we have effectively produced high aspect ratio nanodisks with thicknesses of up to 200 nm using the deep UV lithography technique, facilitating the large area patterning essential for spintronic applications. Initially, nanotrenches were etched into the Si substrate and subsequently filled with magnetic layers. This innovative approach addresses the challenge of edge roughness commonly encountered in conventional lithographic processes for nanostructures. We have performed a detailed investigation on the evolution of spin textures and their effect on spin dynamics of large area permalloy nanodisk of diameter 450 nm with

increasing thickness from 20 to 200 nm. Micromagnetic simulations substantiate our experimental findings. The magnetization reversal studies reveal that the nucleation and annihilation fields of the nanodisks are found to increase with the thickness. The increase in thickness leads to an increase in vortex core diameter and a non-zero OOP magnetization near the peripheral region for t = 170, 200 nm nanodisks. We found that the magnetization configuration of surface layers appears to be mirror images of one another. FMR investigations reveal that the CM frequency increases with increasing thickness. The spatial mode profiles of nanodisks with t > 50 nm exhibit a mirror symmetry in their amplitude between the top and bottom surfaces. Our results offer a novel pathway for large-area patterning techniques with high aspect ratio nanostructures and shed light on the evolution of complex spin textures and spin dynamics, which are critical for developing spintronic devices.

Supporting information

Supporting information is available.

- Simulated magnetization configuration of 200nm-thick-nanodot as a function of the applied field; Simulated hysteresis curves for different thicknesses.

Author information

Corresponding authors

Arabinda Haldar- Department of Physics, Indian Institute of Technology Hyderabad, Kandi 502284, Telangana, India. Email: arabinda@phy.iith.ac.in

Adekunle Olusola Adeyeye- Department of Electrical and Computer Engineering, National University of Singapore, Singapore 117576

Department of Physics, Durham University, South Road, Durham DH1 3LE, United Kingdom. Email: adekunle.o.adeyeye@durham.ac.uk

Authors

M S Devapriya- Department of Physics, Indian Institute of Technology Hyderabad, Kandi 502284, Telangana, India

Xue Zhou- Department of Electrical and Computer Engineering, National University of Singapore, Singapore 117576

Acknowledgments

AH would like to thank the funding under the Core Research Grant (CRG/2022/004492), Science and Engineering Research Board (SERB), India. AOA would like to acknowledge the funding from the Royal Society and Wolfson Foundation. We thank Dr. Navab Singh for providing the initial DUV template, which was used to develop the process and fabricate the Py samples. AH would like to acknowledge the DST - FIST facility, VSM at the Department of Physics, IIT Hyderabad (Project No: SR/FST/PSI-215/2016).

Notes

The authors declare no competing financial interest.

References:

(1) Allwood, D. A.; Xiong, G.; Faulkner, C. C.; Atkinson, D.; Petit, D.; Cowburn, R. P. Magnetic Domain-Wall Logic. *Science* 2005, *309* (5741), 1688–1692.

(2) Parkin, S. S. P.; Hayashi, M.; Thomas, L. Magnetic Domain-Wall Racetrack Memory. *Science* 2008, *320* (5873), 190–194.

(3) Atkinson, D.; Allwood, D. A.; Xiong, G.; Cooke, M. D.; Faulkner, C. C.; Cowburn, R. P. Magnetic Domain-Wall Dynamics in a Submicrometre Ferromagnetic Structure. *Nat Mater* **2003**, *2* (2), 85–87.

(4) Yang, S. H.; Ryu, K. S.; Parkin, S. Domain-Wall Velocities of up to 750 m s-1 Driven by Exchange-Coupling Torque in Synthetic Antiferromagnets. *Nat Nanotechnol* **2015**, *10* (3), 221–226.

(5) Rothman, J.; Kläui, M.; Lopez-Diaz, L.; Vaz, C. A. F.; Bleloch, A.; Bland, J. A. C.; Cui, Z.; Speaks, R. Observation of a Bi-Domain State and Nucleation Free Switching in Mesoscopic Ring Magnets. *Phys Rev Lett* **2001**, *86* (6), 1098–1101.

(6) Kläui, M.; Vaz, C. A. F.; Lopez-Diaz, L.; Bland, J. A. C. Vortex Formation in Narrow Ferromagnetic Rings. *J. Phys.: Condens. Matter* **2003**, *15*, 985–1023.

(7) Zhu, X.; Zhu, J. G. A Vertical MRAM Free of Write Disturbance. *IEEE Trans Magn* **2003**, *39* (5 II), 2854–2856.

(8) Miller, M. M.; Prinz, G. A.; Cheng, S. F.; Bounnak, S. Detection of a Micron-Sized Magnetic Sphere Using a Ring-Shaped Anisotropic Magnetoresistance-Based Sensor: A Model for a Magnetoresistance-Based Biosensor. *Appl Phys Lett* **2002**, *81* (12), 2211–2213.

(9) Zhu, J. G.; Zheng, Y.; Prinz, G. A. Ultrahigh Density Vertical Magnetoresistive Random Access Memory. *J Appl Phys* **2000**, *87* (9 III), 6668–6673.

(10) Gubbiotti, G.; Madami, M.; Tacchi, S.; Carlotti, G.; Tanigawa, H.; Ono, T.; Giovannini, L.; Montoncello, F.; Nizzoli, F. Splitting of Spin Excitations in Nanometric Rings Induced by a Magnetic Field. *Phys Rev Lett* **2006**, *97* (24), 247203.

(11) Podbielski, J.; Giesen, F.; Grundler, D. Spin-Wave Interference in Microscopic Rings. *Phys Rev Lett* **2006**, *96* (16), 167207.

(12) Goiriena-Goikoetxea, M.; Guslienko, K. Y.; Rouco, M.; Orue, I.; Berganza, E.; Jaafar, M.; Asenjo, A.; Fernández-Gubieda, M. L.; Fernández Barquín, L.; García-Arribas, A. Magnetization Reversal in Circular Vortex Dots of Small Radius. *Nanoscale* **2017**, *9*, 11269–11278.

(13) Cowburn, R. P. Magnetic Nanodots for Device Applications. *J Magn Magn Mater* **2002**, *242–245* (PART I), 505–511.

(14) Van Waeyenberge, B.; Puzic, A.; Stoll, H.; Chou, K. W.; Tyliszczak, T.; Hertel, R.; Fähnle, M.; Brückl, H.; Rott, K.; Reiss, G.; Neudecker, I.; Weiss, D.; Back, C. H.; Schütz, G. Magnetic Vortex Core Reversal by Excitation with Short Bursts of an Alternating Field. *Nature* **2006**, *444* (7118), 461–464.

(15) Tarequzzaman, M.; Böhnert, T.; Decker, M.; Costa, J. D.; Borme, J.; Lacoste, B.; Paz, E.; Jenkins, A. S.; Serrano-Guisan, S.; Back, C. H.; Ferreira, R.; Freitas, P. P. Spin Torque Nano-Oscillator Driven by Combined Spin Injection from Tunneling and Spin Hall Current. *Commun Phys* **2019**, *2* (1), 20.

(16) Fernández-Pacheco, A.; Streubel, R.; Fruchart, O.; Hertel, R.; Fischer, P.; Cowburn, R. P. Three-Dimensional Nanomagnetism. *Nat Commun* **2017**, *8* (1), 15756.

(17) Fischer, P.; Sanz-Hernández, D.; Streubel, R.; Fernández-Pacheco, A. Launching a New Dimension with 3D Magnetic Nanostructures. *APL Mater* **2020**, *8* (1), 010701.

(18) Dobrovolskiy, O. V.; Bunyaev, S. A.; Vovk, N. R.; Navas, D.; Gruszecki, P.; Krawczyk, M.; Sachser, R.; Huth, M.; Chumak, A. V.; Guslienko, K. Y.; Kakazei, G. N. Spin-Wave Spectroscopy of Individual Ferromagnetic Nanodisks. *Nanoscale* **2020**, *12* (41), 21207–21217.

(19) May, A.; Hunt, M.; Van Den Berg, A.; Hejazi, A.; Ladak, S. Realisation of a Frustrated 3D Magnetic Nanowire Lattice. *Commun Phys* **2019**, *2* (1), 13.

(20) Sahoo, S.; Mondal, S.; Williams, G.; May, A.; Ladak, S.; Barman, A. Ultrafast Magnetization Dynamics in a Nanoscale Three-Dimensional Cobalt Tetrapod Structure. *Nanoscale* **2018**, *10*, 9981.

(21) Kumar, D.; Lupo, P.; Haldar, A.; Adeyeye, A. O. Unconventional Spin Distributions in Thick Ni80Fe20 Nanodisks. *Appl Phys Lett* **2016**, *108* (19), 192404.

(22) Zhou, X.; Kumar, D.; Maksymov, I. S.; Kostylev, M.; Adeyeye, A. O. Axially and Radially Quantized Spin Waves in Thick Permalloy Nanodots. *Phys Rev B* **2015**, *92* (5), 054401.

(23) Verba, R. V.; Hierro-Rodriguez, A.; Navas, D.; Ding, J.; Liu, X. M.; Adeyeye, A. O.; Guslienko, K. Y.; Kakazei, G. N. Spin-Wave Excitation Modes in Thick Vortex-State Circular Ferromagnetic Nanodots. *Phys Rev B* **2016**, *93* (21), 214437.

(24) Ding, J.; Kakazei, G. N.; Liu, X.; Guslienko, K. Y.; Adeyeye, A. O. Higher Order Vortex Gyrotropic Modes in Circular Ferromagnetic Nanodots. *Sci Rep* **2014**, *4*, 4796.

(25) Ding, J.; Kakazei, G. N.; Liu, X. M.; Guslienko, K. Y.; Adeyeye, A. O. Intensity Inversion of Vortex Gyrotropic Modes in Thick Ferromagnetic Nanodots. *Appl Phys Lett* **2014**, *104* (19), 192405.

(26) Guslienko, K. Y.; Kakazei, G. N.; Ding, J.; Liu, X. M.; Adeyeye, A. O. Giant Moving Vortex Mass in Thick Magnetic Nanodots. *Sci Rep* **2015**, *5*, 13881.

(27) Kakazei, G. N.; Guslienko, K. Y.; Verba, R. V.; Ding, J.; Liu, X. M.; Adeyeye, A. O. Non-Uniform along Thickness Spin Excitations in Magnetic Vortex-State Nanodots. *Low Temperature Physics* **2020**, *46* (8), 863–868.

(28) Taghipour Kaffash, M.; Bang, W.; Lendinez, S.; Hoffmann, A.; Ketterson, J. B.; Jungfleisch, M. B. Control of Spin Dynamics in Artificial Honeycomb Spin-Ice-Based Nanodisks. *Phys Rev B* **2020**, *101* (17), 174424.

(29) Buess, M.; Knowles, T. P. J.; Höllinger, R.; Haug, T.; Krey, U.; Weiss, D.; Pescia, D.; Scheinfein, M. R.; Back, C. H. Excitations with Negative Dispersion in a Spin Vortex. *Phys Rev B Condens Matter Mater Phys* **2005**, *71* (10), 104415.

(30) Cowburn, R. P.; Koltsov, D. K.; Adeyeye, A. O.; Welland, M. E.; Tricker, D. M. Single-Domain Circular Nanomagnets. *Phys Rev Lett* **1999**, *83* (5), 1042.

(31) Park, J. P.; Eames, P.; Engebretson, D. M.; Berezovsky, J.; Crowell, P. A. Imaging of Spin Dynamics in Closure Domain and Vortex Structures. *Physical Review B* **2003**, *67* (2), 020403(R).

(32) Adeyeye, A. O.; Singh, N. Large Area Patterned Magnetic Nanostructures. *J Phys D Appl Phys* **2008**, *41* (15), 153001.

(33) M. J. D.; D. G. Porter. M. J. D. and D. G. Porter, Interag. Rep. NISTIR 6376, Natl. Inst. Stand. Technol., Gaithersburg, MD. *Interag. Rep. NISTIR 6376, Natl. Inst. Stand. Technol., Gaithersburg, MD (1999)* **1999**.

(34) Boust, F.; Vukadinovic, N. Micromagnetic Simulations of Vortex-State Excitations in Soft Magnetic Nanostructures. *Phys Rev B* **2004**, *70* (17), 172408.

(35) Kumar, D.; Adeyeye, A. O. Techniques in Micromagnetic Simulation and Analysis. *J Phys D Appl Phys* **2017**, *50* (34), 343001.

(36) Yan, M.; Wang, H.; Campbell, C. E. Unconventional Magnetic Vortex Structures Observed in Micromagnetic Simulations. *J Magn Magn Mater* **2008**, *320* (13), 1937–1944.

(37) Guslienko, K. Y.; Novosad, V.; Otani, Y.; Shima, H.; Fukamichi, K. Magnetization Reversal Due to Vortex Nucleation, Displacement, and Annihilation in Submicron Ferromagnetic Dot Arrays. *Phys Rev B* **2001**, *65* (2), 024414.

(38) Talapatra, A.; Adeyeye, A. O. Linear Chains of Nanomagnets: Engineering the Effective Magnetic Anisotropy. *Nanoscale* **2020**, *12*, 20933.

(39) Kittel, C. On the Theory of Ferromagnetic Resonance Absorption. *Physical Review* **1948**, *73* (2), 155.

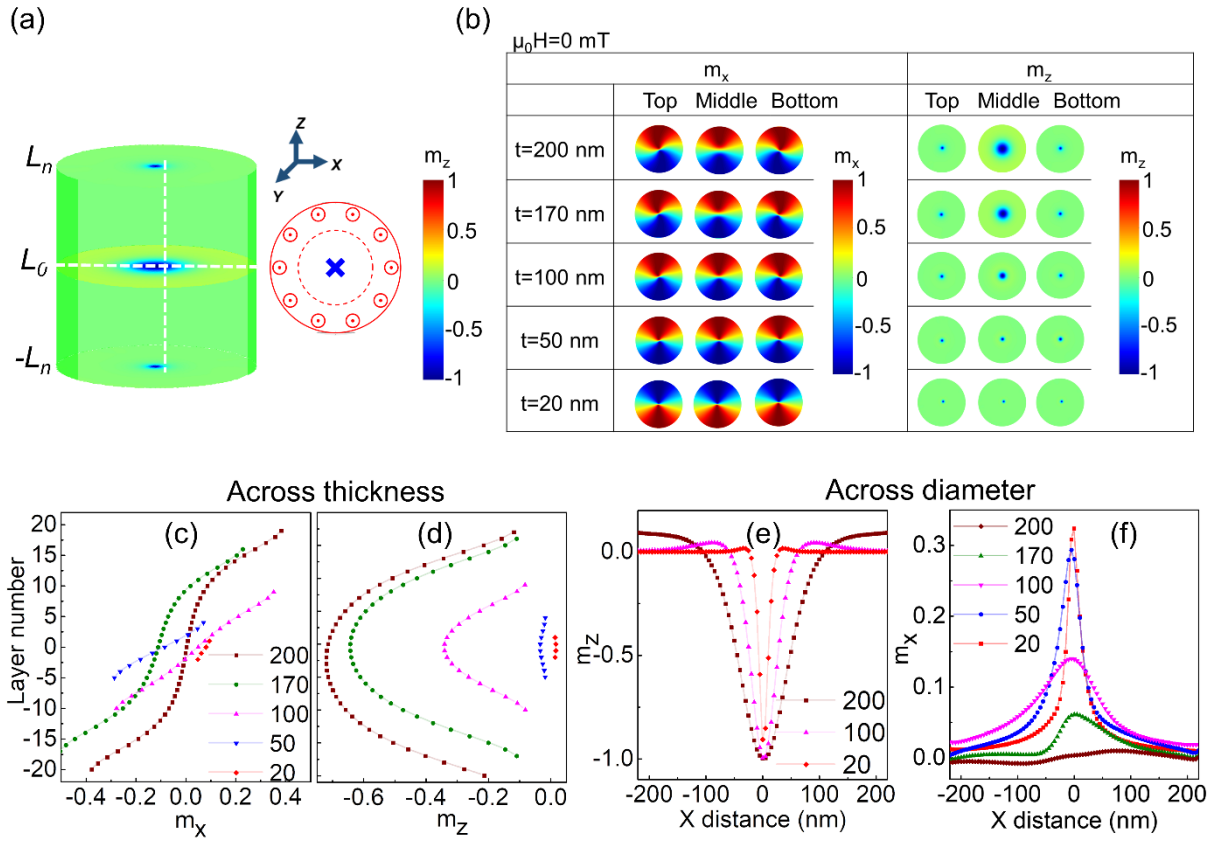

Figure 1. (a) The simulated magnetization configuration of a nanodisk of D = 450 nm and t = 200 nm. The OOP magnetization, m_z, is colour-coded for the nanodisk's top, middle, and bottom layers. L_n, $L_{0,}$ $-L_n$ denotes the top, middle, and bottom layers. The sketch corresponds to the m_z configuration of the middle layer. The cross marks represent the spin pointing down, and the circles indicate the spin pointing up. (b) The simulated IP and OOP magnetization configuration at zero fields for various thicknesses of nanodisk arrays for the top, middle, and bottom layers. The variation of (c) m_x and (d) m_z for a single spin 10 nm away from the center, as a function of layer number (across the vertical dotted line in the cylinder) for different thicknesses. The variation of (e) m_z and (f) m_x along the disk diameter in the middle layer of the disk (represented by the dotted horizontal line in the cylinder).

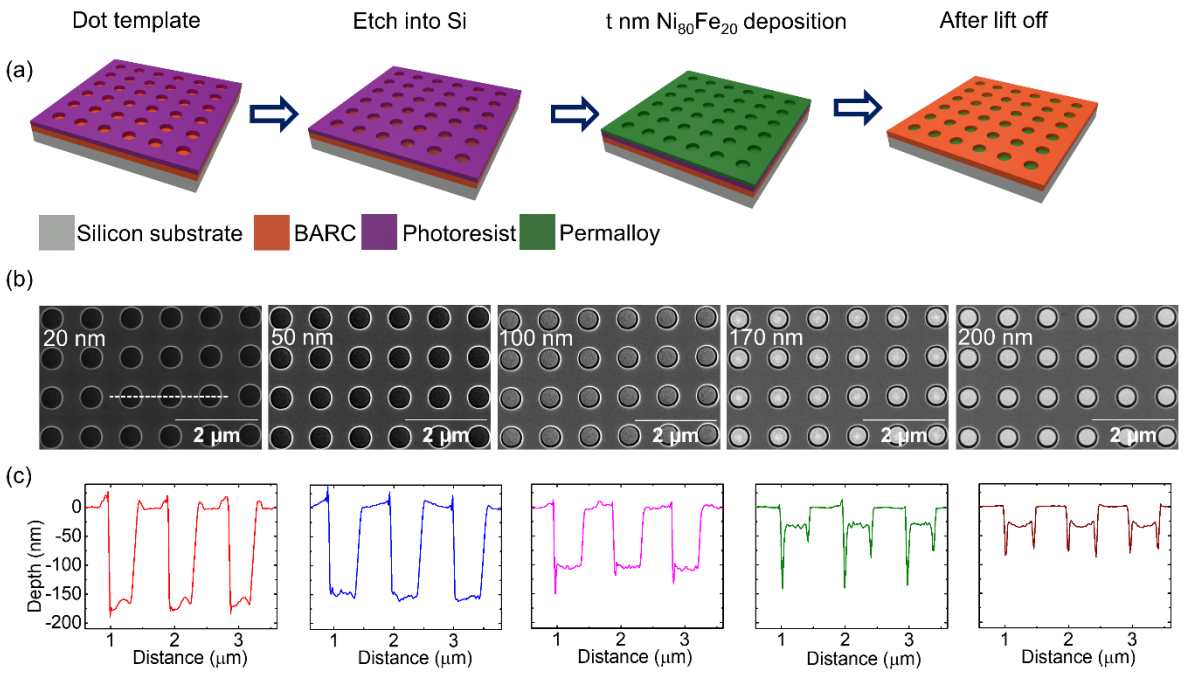

Figure 2. (a) Schematic of the fabrication process, including development of disk template, etching into the silicon substrate, thin film deposition, and lift-off. 2(b) SEM images for the arrays with 20 nm, 50 nm, 100 nm, 170 nm, and 200 nm-thick circular nanodisk arrays. (c) AFM line scans showing the depth profile as indicated by the dashed lines within the SEM images. Note that the height = 0 nm refers to the unetched Si-substrate level, and the negative height values refer to the etched holes in the Si-substrate filled with different thicknesses of Permalloy.

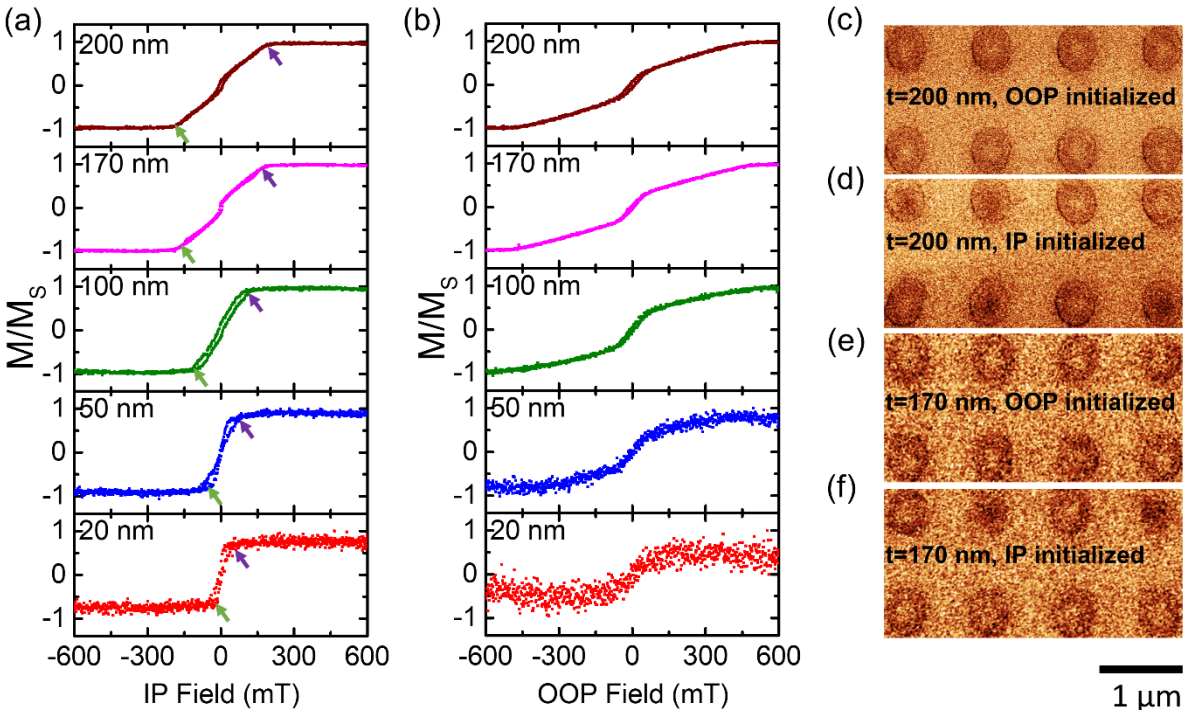

Figure 3. Hysteresis loops for circular nanodisks array of various thicknesses in an (a) IP configuration and (b) OOP configuration as obtained from VSM. The violet and green arrows in (a) represent nucleation and annihilation fields, respectively. MFM images of remanent states of nanodisk arrays with t = 200 nm with field initialization along (c) OOP and (d) IP MFM images of remanent states of nanodisk arrays with t = 170 nm with field along (e) OOP and (f) IP.

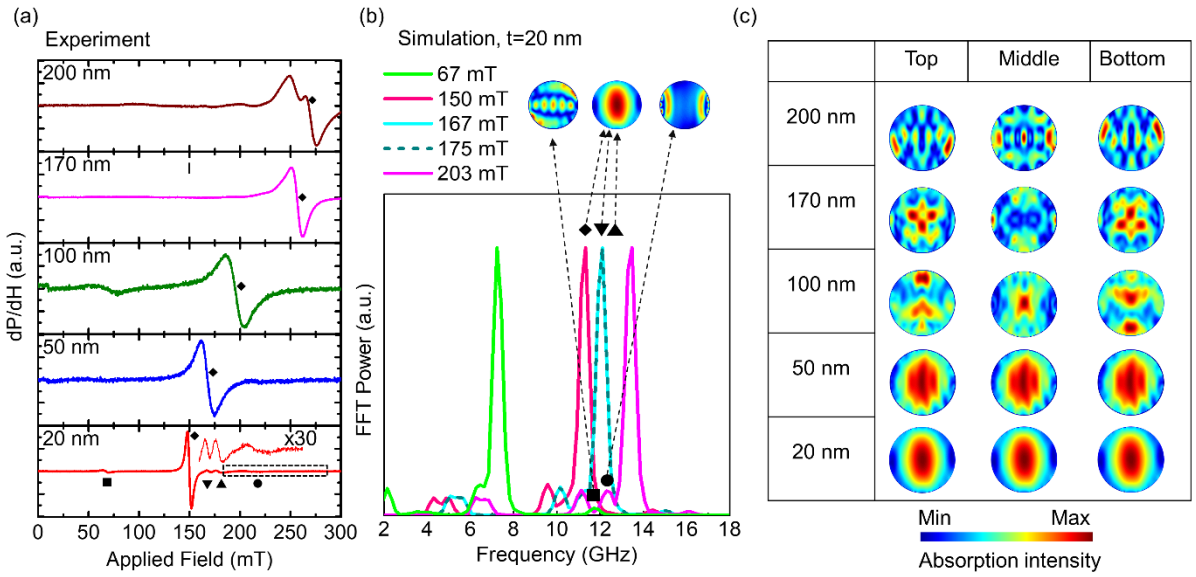

Figure 4. (a) FMR spectra at 12 GHz for nanodisk arrays of different thicknesses. The diamond symbol indicates the CM. (b) Simulated FMR spectra of 20 nm thick nanodisk. The inset shows the corresponding 2D spatial profile of mode amplitudes. Red colour indicates maximum absorption, and blue colour indicates minimum absorption. (c) Normalized 2D spatial profiles at the top, middle, and bottom planes of nanodisks of various thicknesses.

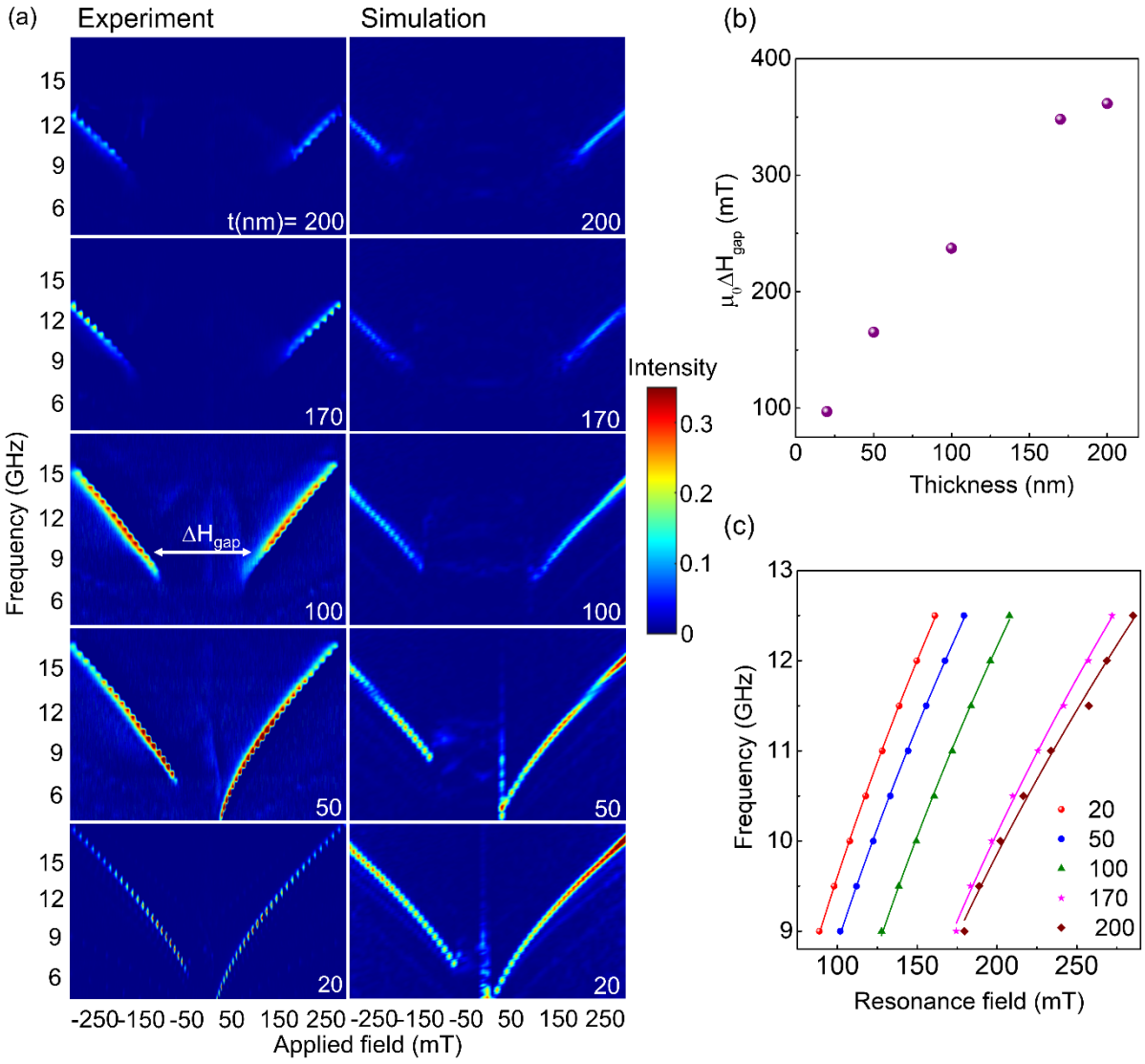

Figure 5. (a) Experimental (left) and simulated (right) two-dimensional FMR contour plots for circular nanodisk arrays of different thicknesses (b) The variation of $\mu_0\Delta H_{gap}$ with the thickness (c) $\mu_0 H_r$ vs frequency plot arrays of different thicknesses. The solid line represents the fit to equation (1).